JOURNAL OF
THE INTERNATIONAL ASSOCIATION
FOR SHELL AND SPATIAL
STRUCTURES

Prof. D. h-C Eng. E. TORROJA, founder

Vol. 58 (2017) No. 4
December n. 194
ISSN: 1028-365X

Journal

VOL. 58 (2017) No. 4
n. 194 December

contents

COVER: *Figures from paper by K. Noda and Y. Kanebako*

IASS Secretariat: CEDEX-Laboratorio Central de Estructuras y Materiales
Alfonso XII, 3; 28014 Madrid, Spain
Tel: 34 91 3357491; Fax: 34 91 3357422; iass@cedex.es; http://www.iass-structures.org
Printed by SODEGRAF ISSN: 1028-365X Depósito legal: M. 1444-1960

TUNABLE FREQUENCY BAND STRUCTURE OF ORIGAMI-BASED MECHANICAL METAMATERIALS

Hiromi YASUDA and Jinkyu YANG

Graduate Research Assistant, Department of Aeronautics and Astronautics, University of Washington
Guggenheim Hall, Seattle, WA 98195, USA, hiromy@uw.edu
Assistant Professor, Department of Aeronautics and Astronautics, The University of Washington
Guggenheim Hall, Seattle, WA 98195, USA, jkyang@aa.washington.edu

Editor's Note: The first author of this paper is one of the four winners of the 2017 Hangai Prize, awarded for outstanding papers that are submitted for presentation and publication at the annual IASS Symposium by younger members of the Association (under 30 years old). It is re-published here with permission of the editors of the proceedings of the IASS Symposium 2017: "Interfaces –Architecture. Engineering. Science" held in September 2017 in Hamburg, Germany.

DOI: https://doi.org/10.20898/j.iass.2017.194.905

ABSTRACT

In this study, we show the formation of frequency band structures in origami-based mechanical metamaterials composed of the Triangulated Cylindrical Origami (TCO). Interestingly, the folding behavior of this structure can exhibit both axial and rotational motions under external excitations. Therefore, these two motions can be strongly coupled with each other, which leads to unique dynamic behavior, particularly wave mixing effects. To analyze the folding behavior of the TCO cells, we model their triangular facets into a network of linear springs. We assemble a 1D chain of multiple TCO unit cells stacked vertically in various arrangements, e.g., changing their stacking sequences and/or orientation angles. We study frequency responses of this system to investigate wave mixing effects between axial and rotational motions under dynamic excitations. This dynamic analysis on the multi-cell structure demonstrates the formation of tunable frequency band structures, which can be manipulated by the arrangement of the unit cells and their initial configurations. By taking advantage of their unique dynamic mechanisms, the origami-based mechanical metamaterials have great potential to be used for controlling structural vibrations in an efficient manner.

Keywords: *origami, mechanical metamaterials, frequency band structure, tunability*

1. INTRODUCTION

Origami can be seen as an effective approach of building 2D or 3D structures from sheets of paper. Depending on the crease patterns of paper sheets, origami shows various shapes and folding behaviors, which can be exploited to construct unique structures with tunable mechanical properties. In particular, for 3D origami structures, one of the well-known origami crease patterns is the Yoshimura pattern, which enables the enhancement of cylindrical structures' bending stiffness [1]. This Yoshimura pattern consists of an identical isosceles triangle facet, and it can be formed as a post-buckled pattern when a thin-walled cylinder is subjected to axial compression. If twist is applied as well as axial compression at the same time, it induces a derivative of the Yoshimura pattern – so-called Triangulated Cylindrical Origami (TCO) (see Fig. 1(a)) – which is composed of non-isosceles triangle surfaces. Researchers have shown versatile kinematics of the TCO structures [2-12]. For example, previous studies have shown that TCO-based structures can exhibit bistable behavior under axial compression [6-8].

Despite their promising features, the dynamic analysis of the TCO structures remains a formidable challenge. This is partly because the facets of the TCO structures are susceptible to planar deformation during folding/unfolding, which makes the dynamic modeling of the TCO extremely complicated. Another reason is that origami, in general, has not been considered as an ideal platform for wave dynamics. Most engineering applications of origami tend to exploit quasi-static deployable nature of origami, while restricting the intrinsic vibrational and wave motions of origami.

In this study, we break the stereotype conception of origami and attempt to employ it as a medium to support the propagation of mechanical waves. Specifically, we approximate the TCO structures into a network of elastic spring elements to suppress the effect of the planar deformation of their facets, while preserving the key features of the TCO cells (see [13] for the validity of this model and its prototypes). For dynamic analysis, we start with modeling a unit cell of the TCO into a two degree-of-freedom (DOF) structure that features axial and torsional motions under perturbations. Next, we connect these TCO unit cells in series to form a 1D system of origami-based mechanical metamaterial. By using theoretical and computational approaches, we verify that this mechanical metamaterial system can exhibit interesting phenomena of wave dynamics, such as wave mixing effect and the formation of frequency bandgap. For example, see Fig. 1(b) for the selective transmission and rejection of specific frequency components as an outcome of the frequency bandgap.

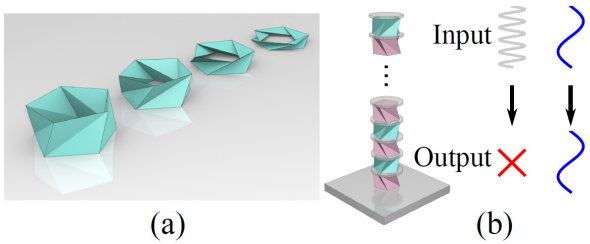

Figure 1: *(a) Folding motion of the Triangulated Cylindrical Origami (TCO). (b) Schematic illustration of TCO-based mechanical metamaterials with allowable and forbidden frequency bands*

The rest of the manuscript is structured as below: In Sec. 2, we describe the geometry of the TCO and we derive the equation of motion for a single TCO unit and a 1D chain of the TCO unit cells. In Sec. 3, we conduct numerical simulations of wave propagation and analyze wave mixing effects and tunable frequency band structures. Lastly, concluding remarks are given in Sec. 4.

2. MODELING OF THE UNIT CELL

To obtain the dynamic folding motion of the TCO unit cell, we introduce a truss-like structure (see Fig. 2) [13,14]. Note that the original TCO model is shown in Fig. 1(a), which has regular polygon cross-sections with n sides (n = 5 in this presented case). For the sake of simplification, we replace the crease lines with linear springs and remove all side surfaces as shown in Fig. 2(a). To determine the initial shape of the TCO, we use the three parameters: initial height (h_0), relative angle (θ_0), and circumradius of the cross-section (R) (see Fig. 2(a-b)). Let u and φ be the axial displacement from the initial height (h_0) and the rotational angle (φ) measured from the initial relative angle (θ_0), respectively. We can obtain height (h) and relative angle (θ) of the TCO unit cell for a deformed shape as follows:

$$h = h_0 - u, \quad \theta = \theta_0 + \varphi \tag{1}$$

See the reference [13] for the detailed descriptions of the geometrical parameters.

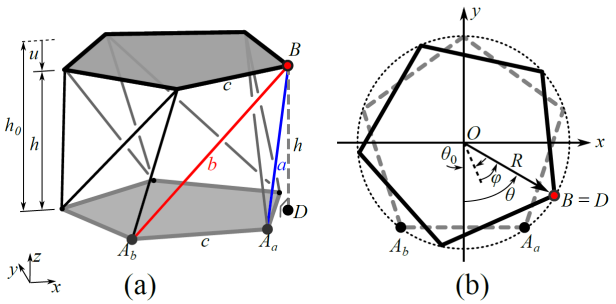

Figure 2: *(a) Side view of the truss-based TCO model with axial displacement (u). (b) Top view of the TCO cell with rotational angle (φ)*

Assuming that the mass of each linear spring element is negligible compared to that of the top surface (pentagonal cross-section in Fig. 2(a)), we can write the equation of motion for the top surface as follows [14]:

$$M\frac{d^2u}{dt^2} + F(u,\varphi) = F_{ex}, \quad J\frac{d^2\varphi}{dt^2} + T(u,\varphi) = T_{ex} \tag{2}$$

where M and J are mass and moment of inertia of the top surface, respectively. The force and torque applied to the top surface by the spring elements are

$$\begin{aligned} F(u,\varphi) &= nK\left(u - h_0\right)\left(2 - \frac{a_0}{a} - \frac{b_0}{b}\right) \\ T(u,\varphi) &= nKR\left\{\left(1 - \frac{a_0}{a}\right)\sin\left(\varphi + \theta_0 - \frac{\pi}{n}\right)\right. \\ &\quad \left. + \left(1 - \frac{b_0}{b}\right)\sin\left(\varphi + \theta_0 + \frac{\pi}{n}\right)\right\} \end{aligned} \tag{3}$$

where a_0 and b_0 are the initial length of linear spring elements a and b, and K is the spring constant for the linear spring elements. Also, F_{ex} and T_{ex} are external force and torque applied to the TCO unit.

Based on the equation of motion for the single TCO unit cell, we design a 1D chain of multiple TCO cells stacked vertically as shown in Fig. 3(a). The equations of motion for j-th unit cell in this system is expressed by

$$\begin{aligned} M_j \frac{d^2 u_j}{dt^2} &= F(u_{j-1}-u_j, \varphi_{j-1}-\varphi_j) \\ &\quad - F(u_j - u_{j+1}, \varphi_j - \varphi_{j+1}) \\ J_j \frac{d^2 \varphi_j}{dt^2} &= T(u_{j-1}-u_j, \varphi_{j-1}-\varphi_j) \\ &\quad - T(u_j - u_{j+1}, \varphi_j - \varphi_{j+1}) \end{aligned} \tag{4}$$

For the first unit cell, equations are expressed by

$$\begin{aligned} M_1 \frac{d^2 u_1}{dt^2} &= -F(u_1-u_2, \varphi_1-\varphi_2) + F_{in} \\ J_1 \frac{d^2 \varphi_1}{dt^2} &= -T(u_1-u_2, \varphi_1-\varphi_2) + T_{in} \end{aligned} \tag{5}$$

In our dynamic analysis, we apply input excitation, force (F_{in}) and torque (T_{in}), to the first unit cell. We solve the nonlinear equations of motion numerically by using the Runge-Kutta method.

In addition to nonlinear equations, we also consider the following linearized equations of motion based on the coefficients from Eq. (3):

$$\begin{aligned} M_j \frac{d^2 u_j}{dt^2} &= \alpha_{uu}\left(u_{j-1}+u_{j+1}-2u_j\right) \\ &\quad + \alpha_{u\varphi}\left(\varphi_{j-1}+\varphi_{j+1}-2\varphi_j\right) \\ J_j \frac{d^2 \varphi_j}{dt^2} &= \alpha_{u\varphi}\left(u_{j-1}+u_{j+1}-2u_j\right) \\ &\quad + \alpha_{\varphi\varphi}\left(\varphi_{j-1}+\varphi_{j+1}-2\varphi_j\right) \end{aligned} \tag{6}$$

where

$$\alpha_{uu} = \frac{\partial F}{\partial u} = nKh_0^2\left(\frac{1}{a_0^2}+\frac{1}{b_0^2}\right)$$

$$\alpha_{u\varphi} = \frac{\partial F}{\partial \varphi} = \frac{\partial T}{\partial u} = -\frac{nKR^2 h_0 \sin\left(\theta_0 - \frac{\pi}{n}\right)}{a_0^2} - \frac{nKR^2 h_0 \sin\left(\theta_0 + \frac{\pi}{n}\right)}{b_0^2}$$

$$\alpha_{\varphi\varphi} = \frac{\partial T}{\partial \varphi} = \frac{nKR^4 \sin^2\left(\theta_0 - \frac{\pi}{n}\right)}{a_0^2} + \frac{nKR^4 \sin^2\left(\theta_0 + \frac{\pi}{n}\right)}{b_0^2} \tag{7}$$

Please note that these coefficients are governed by the initial configurations, i.e., the initial height (h_0) and angle (θ_0).

To conduct eigenvalue analysis on these linearized equations of motion, we use the following ansatz;

$$u_j = ue^{i(kjh_0-\omega t)}, \quad \varphi_j = \varphi e^{i(kjh_0-\omega t)} \tag{8}$$

where k and ω are wave number and angular frequency respectively, and i is the imaginary number. Then we can rewrite Eq. (6) as

$$-\omega^2 \begin{bmatrix} u \\ \varphi \end{bmatrix} = \begin{bmatrix} \frac{\alpha_{uu}}{M_j}\left(e^{-ikh_0}+e^{ikh_0}-2\right) & \frac{\alpha_{u\varphi}}{M_j}\left(e^{-ikh_0}+e^{ikh_0}-2\right) \\ \frac{\alpha_{u\varphi}}{J_j}\left(e^{-ikh_0}+e^{ikh_0}-2\right) & \frac{\alpha_{\varphi\varphi}}{J_j}\left(e^{-ikh_0}+e^{ikh_0}-2\right) \end{bmatrix} \begin{bmatrix} u \\ \varphi \end{bmatrix} \tag{9}$$

Therefore, by solving this equation as an eigenvalue problem, we can calculate the dispersion relation between wave number (k) and frequency (ω).

3. WAVE PROPAGATION IN TCO-BASED MECHANICAL METAMATERIALS

To investigate wave propagation in the 1D chain system composed of TCO unit cells, we conduct numerical simulations as well as eigenvalue

analysis. In this study, we examine the strain waves which are calculated by defining the strain as $\xi_j = (h_{j,0} - h_j) / h_{j,0}$ where $h_{j,0}$ is an initial height of j-th unit cell. Based on the strain field, we apply 2D fast Fourier transform (FFT) and calculate power spectrum to analyze the wave modes in the frequency and wave number domain. For the numerical simulation, we use 80 unit cells, and the bottom (80-th) unit cell is fixed on a rigid wall as shown in Fig. 3(a). Compressive impact (F_{in}) of 110 N is applied to the first unit cell only for the first 1 ms. The numerical parameters used in the dynamic analysis are M = 310 g and $J = 6.37\times10^{-4}$ kg-m^2. The initial height (h_0) of the unit cell is 90 mm, and initial angle (θ_0) is 45°.

Figure 3(b) shows the space-time contour plot of strain waves, and we observe two different wave modes with different group velocities (see arrows in Fig. 3(b)). The wave form at t = 0.15 s is shown in Fig. 3(c), and the smaller amplitude wave denoted by the black arrow in the figure propagates faster than the larger amplitude wave denoted by the red arrow. Figure 3(d) shows the 2D FFT analysis result (surface map, obtained directly by solving Eq. (4)) overlapped with eigenvalue analysis (dotted curves, obtained from Eq. (9)). There is a good agreement between these two results. Here, we also confirm the two branches; one corresponding to the lower mode and the other for the higher mode denoted by black and red arrows in Fig. 3(d), respectively.

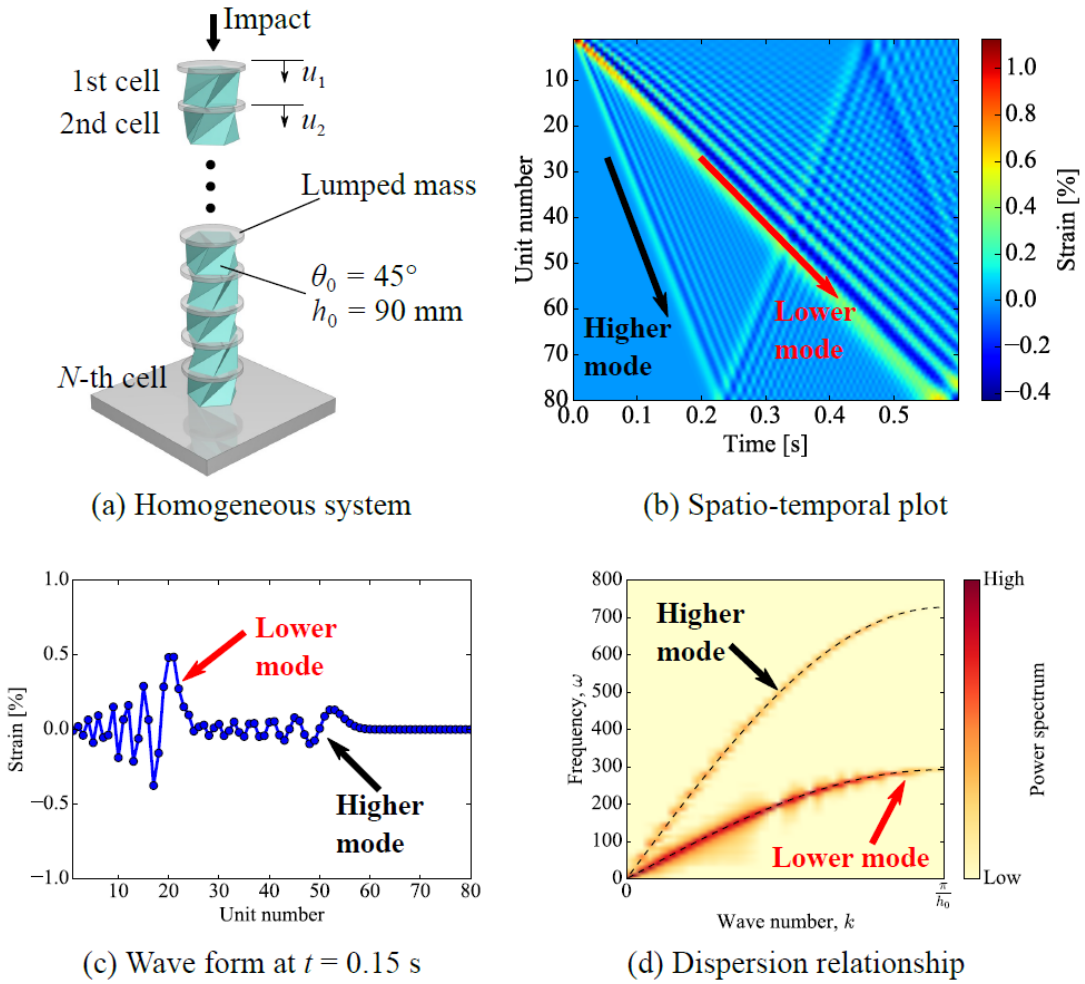

Figure 3: *(a) Illustration of the homogeneous chain of the TCO. All of the unit cells are identical. (b) Spatio-temporal surface plot of strain wave propagation showing two distinctive group velocities. (c) Wave form at t = 0.15 s. (d) Dispersion relationship obtained from 2D FFT applied to (b). Black dashed curves are obtained from the eigenvalue analysis*

These lower and higher modes are formed due to the coupling behavior between axial and rotational motions of the TCO. The modes in a coupled system, where wave dynamics of two channels is coupled, can be manipulated by applying two different inputs to the system [15]. For example, if we use sinusoidal excitation of force and torque as input, we can select a specific mode from the TCO-based structure (see conceptual illustration in Fig. 4(a)). Mathematically, we apply

$$\begin{cases} F_{\text{in}} = F_{\text{amp}} \sin\left(\omega_{\text{in}} t\right) \\ T_{\text{in}} = T_{\text{amp}} \sin\left(\omega_{\text{in}} t\right) \end{cases} \tag{9}$$

where $\omega_{\text{in}} = 200$ rad/s is selected for both force and torque inputs, and $F_{\text{amp}} = 5$ N is used for numerical simulations. Here, we introduce the amplitude ratio defined by $F_{\text{in}}/T_{\text{in}}$ to manipulate coupled wave dynamics. Figure 4(b) shows the strain wave propagation if $F_{\text{in}}/T_{\text{in}} = +20$, and we observe only the lower mode in this case, which is also confirmed by the 2D FFT analysis as shown in Fig. 4(c). On the other hand, if $F_{\text{in}}/T_{\text{in}} = -20$, we obtain the higher mode (see Fig. 4(d,e)). Therefore, by controlling the input excitations, we can manipulate the coupled wave dynamics of the TCO-based structure.

Next, we consider a 1D chain which consists of two different configurations of TCO unit cells and analyze its wave dynamics. We connect two different unit cells ("Unit 1" and "Unit 2" in Fig. 5(a)) in an alternating way to construct a dimer system as shown in Fig 5(a). For the eigenvalue analysis similar to what we have conducted in the homogenous system, we assume the following ansatz

$$\begin{aligned} u_j^{(1)} &= u^{(1)} e^{i(2kjh_0 - \omega t)}, \quad \varphi_j^{(1)} = \varphi^{(1)} e^{i(2kjh_0 - \omega t)} \\ u_j^{(2)} &= u^{(2)} e^{i(2kjh_0 - \omega t)}, \quad \varphi_j^{(2)} = \varphi^{(2)} e^{i(2kjh_0 - \omega t)} \end{aligned} \tag{11}$$

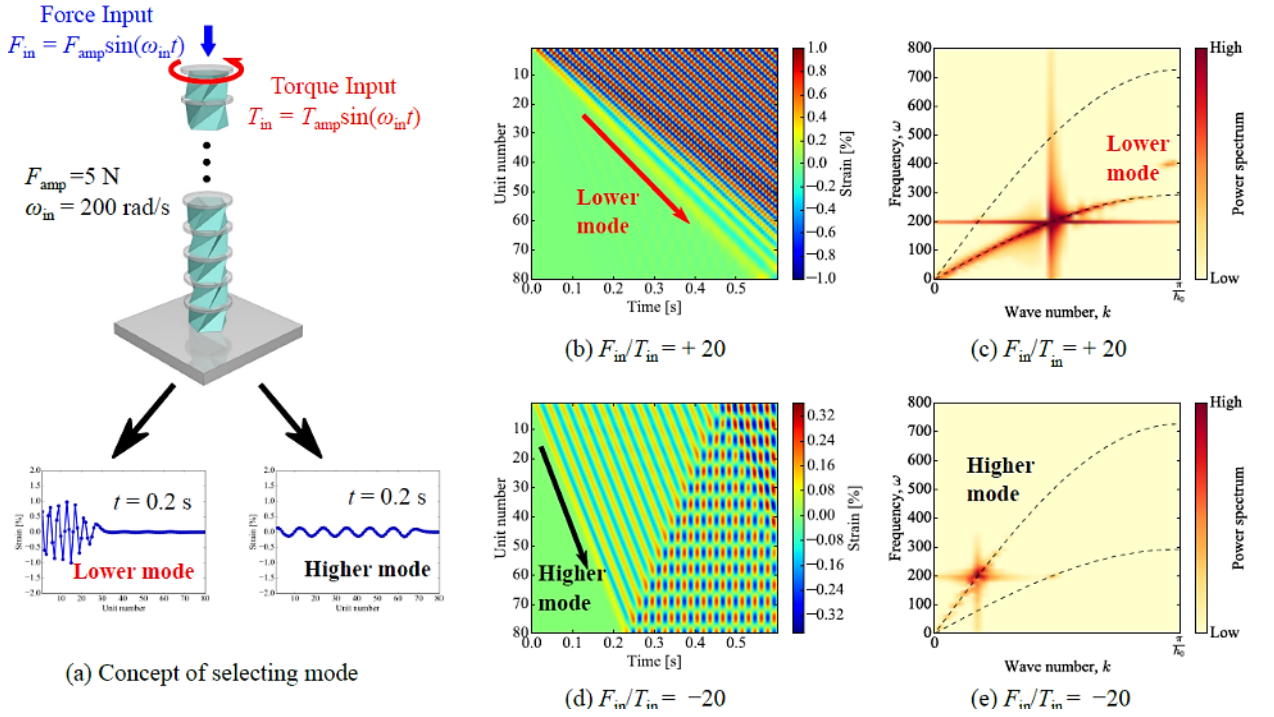

Figure 4: *(a) Conceptual illustration of selecting mode (b) Spatio-temporal surface plot and (c) dispersion relation for $F_{in}/T_{in} = +20$. In this case, the lower mode with the slower group velocity is selected. (d,e) shows the case of $F_{in}/T_{in} = -20$, which triggers only the higher mode with the faster group velocity*

and then we derive the matrix form as follows [14]:

$$-\omega^2\begin{bmatrix} u^{(1)} \\ \varphi^{(1)} \\ u^{(2)} \\ \varphi^{(2)} \end{bmatrix} = \begin{bmatrix} -\dfrac{\alpha_{uu}^{(1)}+\alpha_{uu}^{(2)}}{M_j} & -\dfrac{\alpha_{u\varphi}^{(1)}+\alpha_{u\varphi}^{(2)}}{M_j} & \dfrac{\alpha_{uu}^{(1)}+\alpha_{uu}^{(2)}e^{-2ikh_0}}{M_j} & \dfrac{\alpha_{u\varphi}^{(1)}+\alpha_{u\varphi}^{(2)}e^{-2ikh_0}}{M_j} \\ -\dfrac{\alpha_{u\varphi}^{(1)}+\alpha_{u\varphi}^{(2)}}{J_j} & -\dfrac{\alpha_{\varphi\varphi}^{(1)}+\alpha_{\varphi\varphi}^{(2)}}{J_j} & \dfrac{\alpha_{u\varphi}^{(1)}+\alpha_{u\varphi}^{(2)}e^{-2ikh_0}}{J_j} & \dfrac{\alpha_{\varphi\varphi}^{(1)}+\alpha_{\varphi\varphi}^{(2)}e^{-2ikh_0}}{J_j} \\ \dfrac{\alpha_{uu}^{(1)}+\alpha_{uu}^{(2)}e^{2ikh_0}}{M_j} & \dfrac{\alpha_{u\varphi}^{(1)}+\alpha_{u\varphi}^{(2)}e^{2ikh_0}}{M_j} & -\dfrac{\alpha_{uu}^{(1)}+\alpha_{uu}^{(2)}}{M_j} & -\dfrac{\alpha_{u\varphi}^{(1)}+\alpha_{u\varphi}^{(2)}}{M_j} \\ \dfrac{\alpha_{u\varphi}^{(1)}+\alpha_{u\varphi}^{(2)}e^{2ikh_0}}{J_j} & \dfrac{\alpha_{\varphi\varphi}^{(1)}+\alpha_{\varphi\varphi}^{(2)}e^{2ikh_0}}{J_j} & -\dfrac{\alpha_{u\varphi}^{(1)}+\alpha_{u\varphi}^{(2)}}{J_j} & -\dfrac{\alpha_{\varphi\varphi}^{(1)}+\alpha_{\varphi\varphi}^{(2)}}{J_j} \end{bmatrix}\begin{bmatrix} u^{(1)} \\ \varphi^{(1)} \\ u^{(2)} \\ \varphi^{(2)} \end{bmatrix} \tag{12}$$

where superscript (1) and (2) denote Unit 1 and Unit 2, respectively. From this equation, we calculate the dispersion relation for the dimer system. For numerical parameters, we use the initial angle (θ_0) of 60°/–60° for Unit 1/Unit 2 and the other parameters are the same as those in the previous section.

Figure 5(b) shows the dispersion relation. Here, interestingly, we observe a frequency band gap (i.e., a band of forbidden frequencies), which is created just by changing the direction of the initial angle (θ_0) for even-numbered unit cells compared to the homogeneous system. In addition, if we select different initial angles, we can manipulate this frequency band structure as shown in Fig. 5(c). This implies that the frequency band gap formed in the TCO-based origami structure is highly tunable by altering the initial geometry of the TCO cells. Another notable feature is that the frequency band gap can start from an extremely low frequency. For example, when θ_0 = 90° (i.e., zero-stiffness mode according to [13]), we can completely suppress the formation of the low pass band (see the right inset of Fig. 5(c)). On the other hand, if we employ the Yoshimura pattern (θ_0 = 0°), we observe no frequency band gaps. Such a tunable frequency band structure can be highly useful for engineering devices for adaptive, anti-vibration applications.

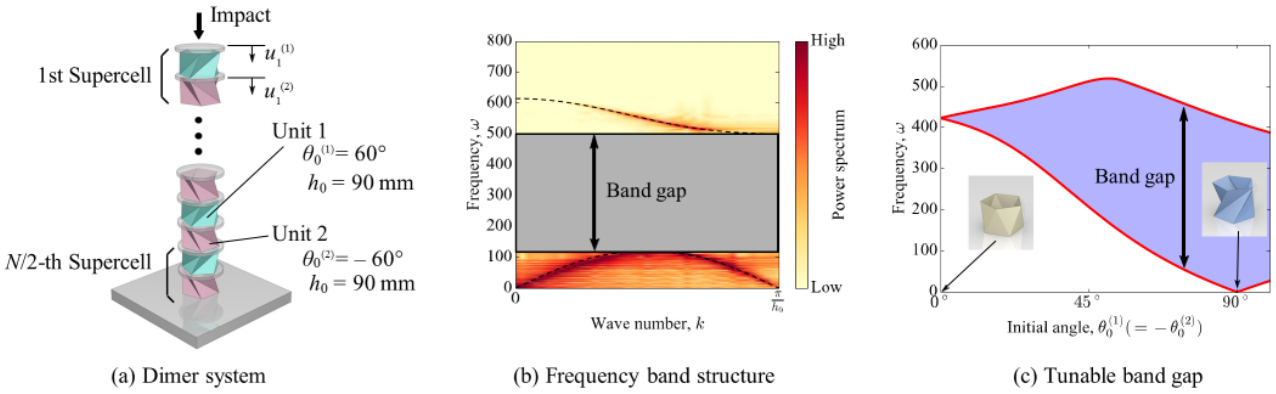

(a) Dimer system (b) Frequency band structure (c) Tunable band gap

Figure 5: *(a) Schematic illustration of the system for a dimer system composed of two different types of the TCO unit cells. (b) Dispersion relationship for the dimer system. The gray shaded area indicates the band gap. (c) Tunable frequency band gap altered by the different initial angles of the Unit 1 and 2*

4. CONCLUSION AND FUTURE WORK

We studied unique wave dynamics of the triangulated cylindrical origami (TCO) structures with the focus on the formation of frequency band structures. For this, we modeled the TCO cells into a network of spring elements, which significantly reduces the complexity of the TCOs' kinematics while preserving their key features. Based on this model, we designed and investigated two different types of TCO-based mechanical metamaterial systems: homogenous and heterogeneous (specifically dimer) configurations. For the homogeneous system, we observe two modes with different group velocities, corresponding to axial and torsional wave modes in the TCO-based metamaterial system. We also find that the application of two different input excitations enables the selection of a specific wave mode. For the dimer system, the system creates a tunable frequency band structure, which can be altered by the initial geometrical configurations of the TCO. By leveraging these unique properties, the TCO-based mechanical metamaterials have great potential to form novel engineering devices, such as deployable space structures and efficient vibration absorbing systems.

ACKNOWLEDGMENTS

We are grateful for the support from the U.S. National Science Foundation (CAREER-1553202) and the Office of Naval Research (N000141410388).

REFERENCES

[1] ***Miura K.***, Proposition of pseudo-cylindrical concave polyhedral shells, In *Proceedings of IASS Symposium on Folded Plates and Prismatic Structures*, 1970, pp. 141-163.

[2] ***Kresling B.***, Plant Design: Mechanical Simulations of Growth Patterns and Bionics, *Biomimetics*, Vol. 3, 1995, pp. 105122.

[3] ***Hagiwara I., Yamamoto C., Tao X., and Nojima T.***, Optimization for crush characteristics of cylindrical origami structure using reversed spiral model, *Transactions of The Japan Society of Mechanical Engineers Series A*, Vol. 70, 2004, pp. 36–42. (in Japanese).
[DOI: 10.1299/kikaia.70.36]

[4] ***Zhao X., Yabo H., and Hagiwara I.***, Optimal design for crash characteristics of cylindrical thin- walled structure using origami engineering, *Transactions of The Japan Society of Mechanical Engineers Series A*, Vol. 76, 2010, pp. 1017.
[DOI: 10.1299/kikaia.76.10]

[5] ***Ishida S., Uchida H., and Hagiwara I.***, Vibration isolators using nonlinear spring characteristics of origami-based foldable structures, *Transactions of The Japan Society of Mechanical Engineers*, Vol. 80, 2014, pp. 1–11. (in Japanese)
[DOI: 10.1299/transjsme.2014dr0384]

[6] ***Jianguo C., Xiaowei D., Ya Z., Jian F., and Yongming T.***, Bistable Behavior of the Cylindrical Origami Structure With Kresling Pattern, *Journal of Mechanical Design*, Vol. 137, 2015, pp. 061406.
[DOI: 10.1115/1.4030158]

[7] ***Jianguo C., Xiaowei D., Yuting Z., Jian F., Ya Z.***, Folding Behavior of a Foldable Prismatic Mast With Kresling Origami Pattern, *Journal of Mechanisms and Robotics*, Vol. 8, 2016, pp. 031004.
[DOI: 10.1115/1.4032098]

[8] ***Ishida S., Uchida H., Shimosaka H., and Hagiwara I.***, Design concepts and prototypes of vibration isolators using bi-stable foldable structures, *Proceedings of the ASME 2015 International Design Engineering Technical Conferences and Computers and Information in Engineering Conference (IDETC/CIE)*, 2015, pp. V05BT08A030.
[DOI: 10.1115/DETC2015-46409]

[9] ***Hunt G. W., and Ario I.***, Twist buckling and the foldable cylinder: an exercise in origami, *International Journal of Non-Linear Mechanics*, Vol. 40, 2005, pp. 833–843.
[DOI: 10.1016/j.ijnonlinmec.2004.08.011]

[10] ***Guest S. D., and Pellegrino S.***, The folding of triangulated cylinders, Part I: Geometric considerations, *Journal of Applied Mechanics*, Vol. 61, 1994, pp. 773–777.
[DOI: 10.1115/1.2901553]

[11] ***Guest S. D., and Pellegrino S.***, The folding of triangulated cylinders, part II: the folding process, *Journal of Applied Mechanics*, Vol. 61, 1994, pp. 778–783.
[DOI: 10.1115/1.2901554]

[12] ***Guest S. D., and Pellegrino S.***, The Folding of Triangulated Cylinders, Part III: Experiments, *Journal of Applied Mechanics*, Vol. 63, 1996, pp. 77–83.
[DOI: 10.1115/1.2787212]

[13] ***Yasuda H., Tachi T., Lee M., and Yang J.***, Origami-based tunable truss structures for non-volatile mechanical memory operation, *Nature Communications*, 8, 2017, pp. 962.
[DOI: 10.1038/s41467-017-00670-w]

[14] ***Yasuda H., Lee M., and Yang J.***, Tunable static and dynamic behavior of triangulated cylindrical origami, In *Proceedings of the IASS annual Symposium* 2016, 2016, pp. 2518-6582.

[15] ***Lee G. Y., Chong C., Kevrekidis P. G., and Yang J.***, Wave mixing in coupled phononic crystals via a variable stiffness mechanism, *Journal of the Mechanics and Physics of Solids*, Vol. 95, 2016, pp. 501-516.
[DOI: 10.1016/j.jmps.2016.06.005]